Investigating grain growth in disks around southern T Tauri stars at millimetre wavelengths

Author/Contributor:
Wright, Christopher; Burton, Michael; Van Dishoeck, Ewine; van Langevelde, Huib-Jan; Wilner, David; Hughes, Annie; Lommen, Dave; Maddison, Sarah; Jorgensen, Jes; Bourke, Tyler

Publication details:
Astronomy & Astrophysics
v. 462
Chapter No. 1
pp. 211-220
0004-6361 (ISSN)

Publication Date:
2007

Publisher DOI:
http://dx.doi.org/10.1051/0004-6361:20066255

Astronomy & Astrophysics manuscript no. atcanew2
June 7, 2006

Investigating grain growth in disks around southern T-Tauri stars at mm wavelengths

Dave Lommen[1], Chris Wright[2], Tyler Bourke[3], Sarah Maddison[4], Jes Jørgensen[3], Ewine van Dishoeck[1], Annie Hughes[4], David Wilner[3], Michael Burton[5], and Huib-Jan van Langevelde[6,1]

[1] Sterrewacht Leiden, Niels Bohrweg 2, 2333 CA Leiden, The Netherlands
[2] School of Physical, Environmental and Mathematical Sciences, UNSW@ADFA, Canberra ACT 2600, Australia
[3] Harvard-Smithsonian Center for Astrophysics, 60 Garden Street, Cambridge, MA 02138, USA
[4] Centre for Astrophysics and Supercomputing, Swinburne University of Technology, PO Box 218, Hawthorn, VIC 3122, Australia
[5] School of Physics, University of New South Wales, Sydney, NSW 2052, Australia
[6] Joint Institute for VLBI in Europe, Postbus 2, 7990 AA Dwingeloo, The Netherlands

Received ?? ; Accepted ??

ABSTRACT

Context. Low-mass stars form with disks around them in which the coagulation of grains may eventually lead to the formation of planets. It is not known when the process of grain growth starts, as models that explain the observations are often degenerate. A way to break this degeneracy is to resolve the sources under study.
Aims. To find evidence for grain growth up to millimeter size in T-Tauri stars.
Methods. The Australia Telescope Compact Array (ATCA) was used to observe 16 T-Tauri stars in the southern constellations Lupus and Chamaeleon at 3 mm. A subsample of 5 sources were observed with the Submillimeter Array (SMA) at 1 mm. Our new data were complemented with data from the literature to estimate the slopes of the spectral energy distributions in the mm regime.
Results. 10 sources were detected at the 3σ level with the ATCA, and all sources that were observed with the SMA were detected at better than 15σ. We find that most of the sources in our sample are resolved which means that the emission is optically thin, so that the mm slope can be directly related to the opacity index. We find that the dust particles in the disks must have grown to millimetre sizes for all detected sources. *DL: note that in principle we can only say "for all detected sources" if we resolve the disk of each and every source, which we do not... The masses of the disks are of the order of* 10^{-2} $M_{\odot}$*, which is comparable to the minimum mass solar nebula.*
Conclusions. The conclusions may go here.

Key words. *circumstellar matter – planetary systems: protoplanetary disks – stars: pre-main-sequence*

1. Introduction

Disks of dust and gas are observed around many young stars. According to the so-called core-accretion model (*DL: ref.? Safronov (1969)?*) planetary systems such as our own Solar System are formed in these circumstellar disks: the solid particles coagulate to form larger grains, which will grow to eventually form planets. The grains mainly consist of carbon and silicates, the former of which are hard to observed. The silicate grains, however, change from amorphous to more crystalline as they grow in size, which was observed by the Infrared Space Observatory (ISO), and more recently by the Spitzer Space Telescope (Malfait et al. 1998; Kessler-Silacci et al. 2006). Although the qualitative picture of grain growth has become much clearer over the last few years (*ref. lab work, e.g., Blum (2006), PPV.*), the quantitative details regarding, e.g., the timescale over which grain growth occurs and how this relates to the disk physical structure (e.g., temperature and density profile) are still under discussion.

A large sample of solar-mass T-Tauri stars and intermediate-mass Herbig-Ae stars have recently been observed with the IRS spectrometer on board the Spitzer Space Telescope, in the context of the "Cores to Disks" (c2d) legacy (Evans et al. 2003) and other programmes. Most sources show 10- and 20-μm amorphous-silicate features (Kessler-Silacci et al. 2006), and confirm and strengthen the results of earlier ISO and ground-based 10-μm observations (e.g., van Boekel et al. 2003; Przygodda et al. 2003) of other sources by extending them to lower-mass objects and larger samples. The data indicate a large variety of silicate features, ranging from strongly-peaked silicate bands and steeply-rising spectral-energy distributions (SEDs) to "boxy" silicate profiles and flat SEDs. The boxy features with low

Send offprint requests to: Dave Lommen,
e-mail: dave@strw.leidenuniv.nl

feature-to-continuum ratios are interpreted as grain growth to μm size (Bouwman et al. 2001).

One possible explanation for the different spectra and SEDs is that grain growth and the shape of the disk are related, in particular whether the disk has a "flaring" or "self-shadowed" disk geometry (Dullemond & Dominik 2004). In these models, the larger, more massive dust grains will settle to the midplane of the disks as the grains grow, and the initially flared disks evolve into the geometrically somewhat flatter self-shadowed disks. To what extent this process is related to the age of the star is still under debate; there are indications that some young stellar objects evolve more quickly than others. The Dullemond & Dominik (2004) models predict that the slopes of the SEDs in the mm-wavelength range will become shallower as the grains in the disk grow to millimetre (mm) and subsequently centimetre (cm) and larger sizes. It is therefore necessary to observe these sources at larger wavelengths than the infrared. Another advantage is that the mm data probe the entire disk including the cold midplane whereas the infrared observations only probe the hot surface layer in the inner AU. However, a shallow mm slope in itself is not enough evidence for grain growth in the disks, since an excess flux at long wavelengths may also be caused by a very small, optically thick disk. To break this degeneracy one needs to resolve the disks to determine their actual sizes, which can only be done by interferometric observations.

Considerable progress has been made in this field over the last several years. Wilner et al. (2000) resolved the inner disk of the classical T-Tauri star TW Hya in dust emission at 7 mm using the Very Large Array (VLA). Calvet et al. (2002) did extensive modelling of the SED of this source and showed that the dust grains in the disk must have grown to sizes of at least ~ 1 cm. Wilner et al. (2003) used the Australia Telescope Compact Array[1] (ATCA) to study TW Hya at 3 mm and found that a passive two-layer disk (Chiang & Goldreich 1999) provides a reasonable model to explain the observations. 10 T-Tauri stars in the Taurus-Auriga star-forming regions were resolved at 7 mm with the VLA by Rodmann et al. (2006) and the majority of these show strong evidence for grain growth to at least millimetre-sized dust. Natta et al. (2004) analysed interferometric observations of a total of 9 pre-main-sequence stars and find that the dust in some of the disks may even have grown to over metre sizes.

Assuming that as grains grow the gas also depletes, another way of determining disk lifetimes, as well as their chemistry and kinematics, is to observe the molecular component. Wilner et al. (2003) used the ATCA to observe TW Hya and HD100546 in HCO^+ $J = 1$–0. HCO^+ was detected in the former but not in the latter, from which Wilner et al. inferred that HD100546 may be more evolved than TW Hya. van Kempen et al. (2006) detected a double-peaked CO line in IM Lup using the James Clerk Maxwell Telescope (JCMT). The double peak is a clear indication of a rotating disk. *DL: more references on line data?*

We have used the ATCA to observe a sample of 16 southern T-Tauri stars, 5 in Lupus and 9 in Chamaeleon, at 3-mm continuum. The sources IM Lup and WW Cha were also observed in spectral-line mode to detect HCO^+. The observations of the Lupus sources were followed up with 1-mm observations using the SubMillimeter Array[2] (SMA). The sample and the observations are described in Sect. 2. The basic results are presented in Sect. 3 and further discussed in Sect. 4. We draw some conclusions in Sect. 5. *To be updated...*

2. Observations

2.1. Source selection

The ATCA was used to observe 16 southern T-Tauri stars (listed in Table 1) at 3.3 mm. The sources were selected to overlap with the sample observed in the c2d programme as much as possible. Furthermore we selected sources with strong 1-mm fluxes (Henning et al. 1993; Nuernberger et al. 1997) to improve the chances of detection at 3 mm.

The distances to these pre-main-sequence stars are not well constrained (see, e.g., Comerón in prep.; van Kempen et al. 2006, for discussions on the distances to the Lupus clouds). The distances used here are 150 pc to Lupus I (HT Lup, GW Lup) and Lupus II (IM Lup, RU Lup), 200 pc to Lupus III (HK Lup), and 178 pc to the Chamaeleon sources (Whittet et al. 1997).

An overview of the ATCA and SMA observations is given in Table 2. *DL: maybe we should just throw out Table 2, because it doesn't seem to add anything useful...*

2.2. ATCA observations

Observations were carried out in July 2003, October 2004, and August 2005. All sources were observed at double-side-band continuum, and single-side-band observations were carried out to detect the HCO^+ (1-0) line in WW Cha and IM Lup. The continuum data were recored in two 32-channel bands with widths of 96 MHz, and line data were recorded in one 512-channel band with a width of 8 MHz, resulting in a velocity resolution of $\sim$0.1 km s^{-1} and a velocity coverage of $\sim$20 km s^{-1}. The effective (u, v) coverage had spacings between 6 and 33, 13 and 30, and 10 and 76 kλ in 2003, 2004, and 2005, respectively. The data were calibrated and reduced with the MIRIAD package (Sault et al. 1995). The quasars PKS 1622-297 and PKS 1057-797 served as gain calibrators for the Lupus and Chamaeleon sources, respectively, and the absolute fluxes were calibrated on Mars or Uranus. The calibration is expected to have an uncertainty of $\sim$20 %. The correlator passbands were calibrated on the quasars PKS 0537-441 and PKS 1253-055.

The phase centre was usually offset by $\sim$2 beam sizes to avoid interference problems. There was some overlap in the samples that were observed in the three runs. It turned out that the 2004 data were unusable due to technical problems at the

[1] The Australia Telescope Compact Array is part of the Australia Telescope which is funded by the Commonwealth of Australia for operation as a National Facility managed by CSIRO

[2] The SubMillimeter Array is a joint project between the Smithsonian Astrophysical Observatory and the Academia Sinica Institute of Astronomy and Astrophysics and is funded by the Smithsonian Institution and the Academia Sinica.

Table 1. Source list of sources observed with ATCA.

Source	Spectral type	L_* ($L_\odot$)	Dist. (pc)	Refs.[a]	When observed[b]	Other names[c]
SY Cha	M0	0.35	178 ± 18	1, 9, 12	2005	IRAS 10557-7655, SZ 3, HBC 565, Cha T4
CR Cha	K2	2.7	178 ± 18	1, 12	2003†; 2005	IRAS 10578-7645, SZ 6, HBC 244, Cha T8
CS Cha	K4	1.32	178 ± 18	2, 9, 12	2003†; 2005	IRAS 11011-7717, SZ 9, HBC 569, Cha T11
DI Cha	G2V	8.7	178 ± 18	1, 12	2005	KG 6, IRAS 11059-7721, SZ 19, HBC 245, Cha T26
KG 28	K7[c]		178 ± 18	3, 12	2005	SZ 22, Cha T29
Glass I[d]	K4	1.3	178 ± 18	5, 9, 12	2005	IRAS 11068-7717, Cha T33
KG 49	M5[c]		178 ± 18	6, 12	2004†; 2005	IRAS 11072-7727
WW Cha	K5	2.2	178 ± 18	2, 9, 12	2003†; 2004†; 2005	IRAS 11083-7618, SZ 34, HBC 580, Cha T44
XX Cha	M1	0.10	178 ± 18	2, 9, 12	2005	IRAS 11101-7603, SZ 39, HBC 586, Cha T49
T Cha	G2	$1.4^{+0.8}_{-0.5}$	178 ± 18	10, 11, 12	2003†; 2005	IRAS 11547-7904
KG 87			178 ± 18	12	2004†	
HT Lup[e]	K2	6.0	150 ± 20	1, 8, 13	2003†; 2005	IRAS 15420-3408, SZ 68, HBC 248
GW Lup	M2	0.23	150 ± 20	8, 13	2003†; 2005	IRAS 15435-3421, SZ 71, HBC 249
IM Lup	M0	1.3	150 ± 20	8, 13	2003†; 2005	IRAS 15528-3747, SZ 82, HBC 605
RU Lup	K7-M0	2.1	150 ± 20	8, 13	2003†; 2005	IRAS 15534-3740, SZ 83, HBC 251
HK Lup	M0	0.62	200 ± 20	8, 13	2003	IRAS 16050-3857, SZ 98, HBC 616

[a] (1) Herbig & Kameswara Rao (1972); (2) Alcala et al. (1995); (3) Kenyon & Gómez (2001); (4) de Winter et al. (2001); (5) Gauvin & Strom (1992); (6) Cambresy et al. (1998)†; (7) Kwok et al. (1997); (8) Hughes et al. (1994); (9) Lawson et al. (1996); (10) van den Ancker et al. (1998); (11) Shevchenko et al. (1991); (12) Whittet et al. (1997); (13) Comerón (in prep.)

[b] The observations marked with a † were not used in the analysis.

[c] Catalogue names: KG = [KG2001] (Kenyon & Gómez 2001), IRAS = Infrared Astronomical Satellite, SZ = Southern Zwicky (Rodgers et al. 1978), HBC = Herbig+Bell Catalog (Herbig & Bell 1988), Cha T = Assoc Chamaeleon T (Henize & Mendoza 1973).

[d] From photometry.

[e] This source is a binary with a separation of 2.″4; the spectrum quoted is that of component A.

[f] This source is a binary in 2MASS K-band images with a separation < 3″. The spectrum quoted includes both sources.

time of the observations. The 2003 and 2005 data were consistent. Since there were only 3 antennae with 3-mm receivers available in 2003, compared with 5 in 2005, and the beam resulting from the 2003 observations was relatively large and elongated, it was decided to use only the 2005 data in our analysis. The exception is HK Lup, which was not observed in 2005, and 2003 data are used. The source KG 87 was only observed in 2004 and will not be further discussed in this work, leaving a total of 15 sources.

2.3. SMA observations

The 5 Lupus sources in our sample were observed at 216 and 226 GHz with the SMA on 28 April 2006. The data from both sidebands, with a bandwidth of 1.5 GHz each, were combined. The (u, v) coverage of 4 to 53 kλ yielded a rather elongated synthesized beam of $\sim 9 \times 2.5$ arcsec (natural weighting) due to the low elevation of the sources as seen from Mauna Kea and the relatively short integration time of $\sim$ 30 minutes per source. The raw visibility data were calibrated and flagged with MIR, and the calibrated visibility data were analysed with Miriad. The gains were calibrated on the quasar PKS 1622-297, and the absolute fluxes and correlator passbands were calibrated on Uranus with an expected uncertainty of ∼20 %. Antenna 7 consistently showed a lower amplitude than the other antennae for no clear reason and was excluded in the analysis.

3. Results

From the 15 sources that were observed with ATCA in 2003 and 2005 10 were detected at the 3σ level. Point sources were fitted in the (u, v) plane, the results of which are presented in Table 3. Those sources that were observed at 5σ or better are shown in Fig. 1, overplotted on 2MASS images. The positions of the infrared sources and the mm peaks agree very well.

Table 4 presents the results of the SMA observations of the Lupus sources, which were all detected at better than 15σ. If the results of the point-source fits in the (u, v) plane are compared to 1.3-mm single-dish fluxes (Nuernberger et al. 1997, see Table 5), the interferometric fluxes come out 30 to 50 % lower than the single-dish fluxes. Note that the slightly higher frequency at which the SEST observations were taken (230 GHz vs. 221 GHz) already accounts for an increase of the flux by some 12 % due to the mm slope in the SED alone. The remaining excess flux is explained by the fact that a point-source fit underestimates the total flux of an extended source, and by the fact that the larger single-dish beam picks up more extended emission that is mapped out in the interferometric observations. The only source that does not show a large excess in the single-dish observations compared with the interferometric observations is HK Lup, which is explained by the relatively large beam size due to the lack in (u, v) coverage in the 2003 observations.

Table 2. Overview of the observations.

Obs. dates	Freqs. covered (GHz)	Baslines covered (kλ)	# Antennae used
	ATCA		
10 July 2003	89.999, 90.095	8-33	3
11 July 2003	89.999, 90.095	9-33	3
12 July 2003	89.999, 90.095	6-33	3
13 July 2003	89.999, 90.095	6-33	3
14 October 2004	95.000, 97.000	13-30	5
19 August 2005	89.181, 91.456	19-76	5
24 August 2005	89.180, 91.456	12-70	5
	90.000, 90.096	14-75	5
25 August 2005	89.176, 91.456	10-71	5
26 August 2005	89.176, 91.456	12-71	5
28 August 2005	89.176, 91.456	12-71	5
	SMA		
28 April 2006	216.609, 226.154	4-53	8

Table 3. Basic results of ATCA observations at 3.3 mm. Observations are all around 3.3 mm.

Source name	Continuum flux[a] (mJy/beam)	RMS[a] (mJy/beam)	RA[a] (J2000)	Dec.[a] (J2000)	Beam size[b] (arcsec)
SY Cha	< 4.8[b]	1.6	10 56 30.4	-77 11 45.0	2.46×2.21
CR Cha	6.2	1.5	10 59 06.9	-77 01 39.7	2.54×2.13
CS Cha	5.9	1.5	11 02 24.9	-77 33 35.9	2.44×2.19
DI Cha	< 3.9[b]	1.3	11 07 21.6	-77 38 12.0	2.42×2.21
KG 28	< 3.9[b]	1.3	11 07 57.9	-77 38 50.0	2.40×2.29
Glass I	< 3.0[b]	1.0	11 08 15.1	-77 33 59.0	2.39×2.35
KG 49	11.9	1.5	11 08 38.6	-77 43 52.1	2.42×2.24
WW Cha	25.9	1.2	11 10 00.0	-76 34 58.0	2.54×2.20
XX Cha	< 4.5[b]	1.5	11 11 39.7	-76 20 21.0	2.41×2.16
T Cha	6.4	1.0	11 57 13.6	-79 21 31.7	2.48×2.35
HT Lup	8.3	1.1	15 45 12.9	-34 17 30.8	2.41×1.67
GW Lup	8.5	1.9	15 46 44.7	-34 30 36.0	5.33×1.67
IM Lup	8.9	1.3	15 56 09.2	-37 56 06.3	2.27×1.65
RU Lup	12.7	1.0	15 56 42.3	-37 49 16.0	2.31×1.65
HK Lup	7.3	2.1	16 08 22.5	-39 04 46.3	38.20×3.63

[a] Continuum flulx and position are from point-source fits in the (u, v) plane. The RMS is taken from the cleaned image. For sources that were not detected the coordinates of the phase centre are quoted.
[b] Restored beam, using natural weighting.
[c] Quoted value is 3σ upper limit.

3.1. Sources resolved out?

Plots of the amplitude as a function of baseline are presented in Figs. 2 and 3. It is seen that at least some of the detected sources are resolved out. To pursue this observation further, circular gaussians were also fitted to the sources, the results of which are presented in Table 5; the sources not listed in this Table were not detected. We here define a source as being resolved out at the available resolution if the integrated flux of a fitted gaussian is at least 2σ higher than the (peak) flux of a fitted point source. Note that for a point source the peak flux density (in mJy/beam) is the same as the integrated flux (in mJy). According to this definition 5 of the detected sources (KG 49, WW Cha, HT Lup, IM Lup, RU Lup) are resolved by the ATCA, and 3 of the Lupus sources (IM Lup, RU Lup, HK Lup) are resolved by the SMA. (*DL: perhaps change the gaussian sizes in arcsec in Table 5 to disk sizes in AU, using the distances as quoted in Table 1?*) To directly relate the mm slope in an SED to the opacity index an optically-thin disk must be assumed, and this assumption can only be fully justified if the source is resolved.

3.2. Opacity index

The opacity index β (given by $\kappa_\nu \propto \nu^\beta$) can be estimated from the mm slope $\alpha_{\rm mm}$ ($F_\nu \propto \nu_{\rm mm}^\alpha$) in the SED. We calculate $\alpha_{\rm mm}$ from the SEST 1.3-mm fluxes (Nuernberger et al. 1997; Henning et al. 1993) and the integrated fluxes from our gaussian fits to the ATCA 3.3-mm data (Table 5). This way we do account for the extendedness of some of the sources, but not for the potential contribution of ambient material to the single-dish flux. For the sources that were observed with the SMA $\alpha_{\rm mm}$ was

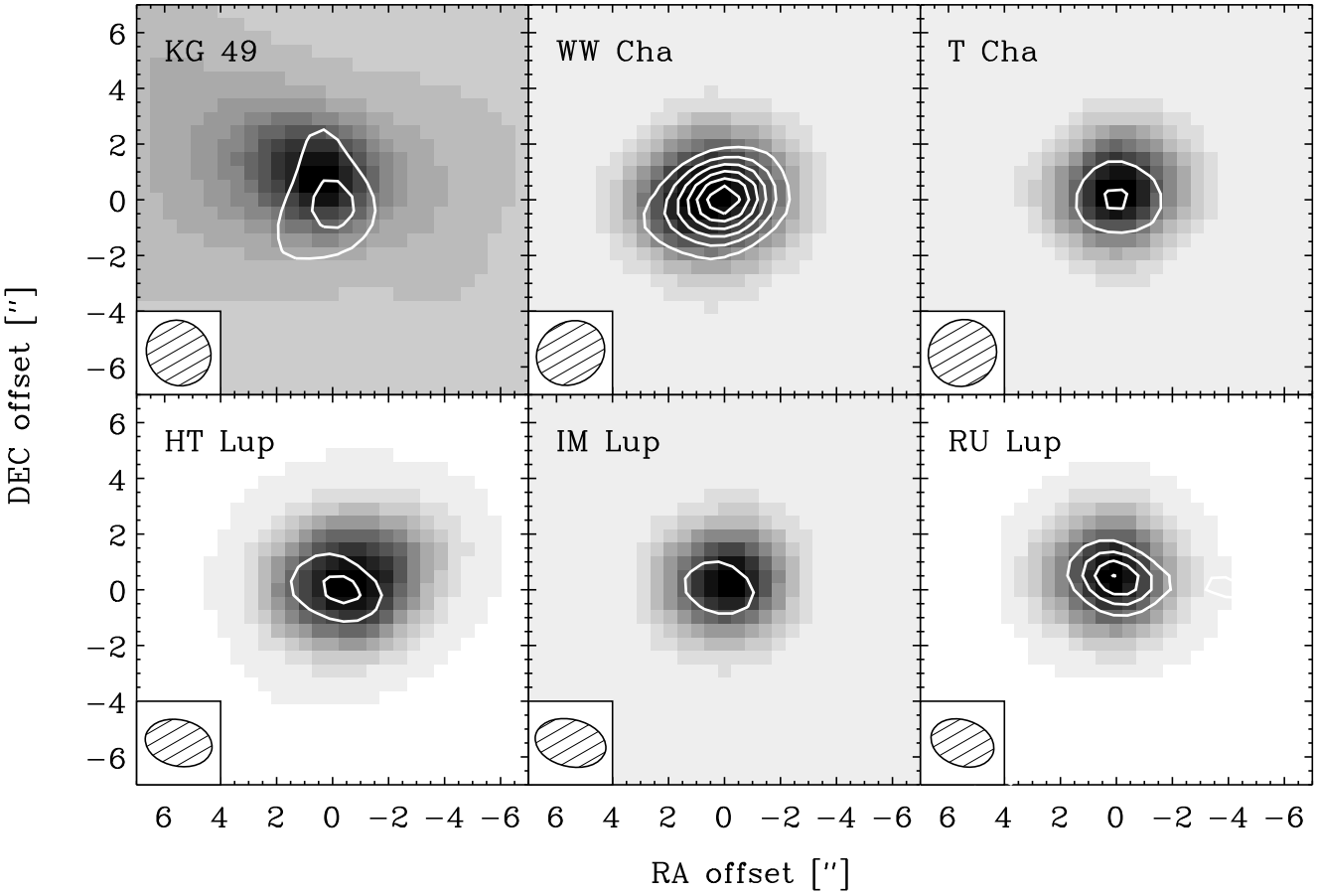

Fig. 1. ATCA images of the λ = 3.3-mm continuum emission (contours), overplotted on 2MASS images (grayscales). Contour levels are drawn at 2, 4, 6, 10, 15, and 20 times the noise level. The positional offsets are with respect to the point-source-fitted coordinates (see Table 3).

Table 4. Basic results of SMA observations at 1.36 mm (221 GHz).

Source name	Continuum flux[a] (mJy/beam)	RMS[a] (mJy/beam)	RA[a] (J2000)	Dec.[a] (J2000)	Beam size[b] (arcsec)
HT Lup	68	3.9	15 45 12.9	-34 17 30.1	8.25 × 2.46
GW Lup	60	3.5	15 46 44.8	-34 30 35.7	9.21 × 2.58
IM Lup	175	4.2	15 56 09.2	-37 56 06.5	8.56 × 2.40
RU Lup	137	4.4	15 56 42.3	-37 49 15.9	8.79 × 2.43
HK Lup	84	3.8	16 08 22.5	-39 04 47.5	11.35 × 2.50

[a] Continuum flux and position are taken from point-source fits in the (u, v) plane. The RMS is taken from the cleaned image.
[b] Restored beam, using natural weighting.

also calculated from the SMA and the ATCA data. It turned out that $\alpha_{\rm mm}$ was overestimated when calculated from SEST and ATCA data whereas for the resolved sources the result remains largely the same. This is beautifully illustrated by Fig. 4, which shows the fluxes from the gaussian fits from this work and the single-dish (sub)mm fluxes from the literature (Weintraub et al. 1989; Nuernberger et al. 1997) for RU Lup. All data points fall very nicely on a line with slope $\alpha_{\rm mm}$ = 2.6, which is exactly the value found from the SEST and ATCA data alone. A best fit between the SMA and ATCA interferometric data points requires $\alpha_{\rm mm}$ = 2.5. From this it is clear that a determination of $\alpha_{\rm mm}$ from the SEST single-dish and the ATCA interferometric data points provides a good value for the (sub)mm slope, at least for this resolved source.

To calculate β we follow the same procedure as Rodmann et al. (2006). First we estimate β from the canonical formula $\beta = \alpha - 2$. Then we correct for optical thickness, so that effectively we use $\beta \approx (\alpha - 2) \times (1 + \Delta)$, where Δ is the ratio of

Table 5. Single-dish fluxes from the literature (Cols. 2, 3) are shown together with results of guassian fits to sources in the (u, v) plane (Cols. 4–7). The mm slopes and the derived opacity indices are shown in Cols. 8 & 9, and the disk masses as calculated from the 3.3-mm flux assuming optically thin disks in Col. 10.

Source name	SEST[a]		SMA 1.36 mm		ATCA 3.3 mm		Mm slope	Opacity index	Disk mass
	Flux (mJy)	RMS (mJy)	Flux (mJy)	Gaussian size (arcsec)	Flux (mJy)	Gaussian size (arcsec)	$\alpha_{\rm mm}$	β	$M_{\rm disk}$ ($M_\odot$)
CR Cha	125	24	-	-	6.1	0.01 ± 27.5	3.1	1.4	0.02
CS Cha	128	46	-	-	8.8	1.65 ± 0.96	2.8	0.9	0.02
KG 49	263	38	-	-	29.5	2.78 ± 0.40	2.3	0.3	0.07
WW Cha	408	29	-	-	33.1	1.32 ± 0.16	2.6	0.7	0.08
T Cha	105	18	-	-	7.0	0.78 ± 1.03	2.8	1.0	0.003
HT Lup	135	15	73	1.01 ± 0.66	12.0	1.40 ± 0.41	2.5	0.6	0.02
GW Lup	106	18	66	1.22 ± 0.48	9.5	0.98 ± 1.22	2.5	0.6	0.009
IM Lup	260	9	199	1.33 ± 0.20	13.1	1.40 ± 0.39	3.1	1.3	0.01
RU Lup	197	7	148	1.02 ± 0.32	15.6	0.99 ± 0.32	2.6	0.8	0.02
HK Lup	84	17	95	1.43 ± 0.38	9.1	2.85 ± 1.70	2.3	0.4	0.009

[a] 1.3-mm single-dish observations from Henning et al. (1993); Nuernberger et al. (1997)

optically thick to optically thin emsission (see Beckwith et al. 1990). For their sample of T-Tauri stars Rodmann et al. (2006) find $\Delta \approx 0.2$, which is the value we also adopt. The results are shown in Table 5. Note that we did not adjust for free-free emission like Rodmann et al. (2006). We estimate the contribution of free-free emission to be $\lesssim 5$ % at 3.3 mm, which makes it neglible compared to the error in the absolute flux calibration.

In Fig. 5 we show the distribution of dust opacity indices for our sample and for that of Rodmann et al. (2006). The results of both samples are very similar, with maybe a small offset to lower values for our sample. (*Probably not statistically significant. How to check?*)

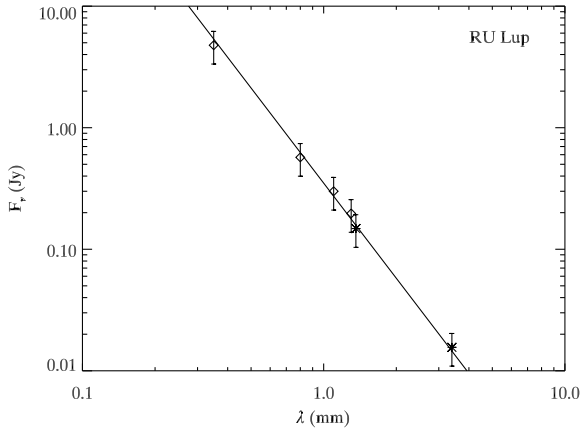

Fig. 4. F_ν vs. λ for RU Lup. Diamonds show fluxes from single-dish observations (JCMT & SEST), asterisks show the values for the interferometric observations from this work. All points fall nicely on a line with $\alpha = 2.6$. This indicates that the contribution of ambient material to the single-dish fluxes can be neglected.

3.3. Disk masses

For optically thin disks the disk mass $M_{\rm d}$ is directly proportianal to the flux F_ν (see, e.g., Hildebrand 1983; Natta et al. 2000):

$$M_{\rm disk} = \frac{F_\nu \Psi D^2}{\kappa_\nu B_\nu(T_{\rm dust})}, \quad (1)$$

where Ψ is the gas-to-dust ratio, D is the distance to the source, κ_ν is the dust opacity and $B_\nu(T_{\rm dust})$ is the brightness at the frequency ν for a dust temperature $T_{\rm dust}$ as given by the Planck function. We have assumed $\Psi = 100$, $T_{\rm dust} = 50$ K, and $\kappa = 0.4$ cm^2 g^{-1} at 3 mm, obtained by extrapolating the opacities presented by Ossenkopf & Henning (1994) and taking an opacity index $\beta = 1$ (see above). The results are presented in Table 5. Note that the mass estimates are quite uncertain, caused mainly by the uncertainties in κ_ν and, for some sources, in D.

3.4. Lines

Both IM Lup and WW Cha were observed in spectral-line mode to try and detect HCO$^+$ J = 1–0 emission. We detected HCO$^+$ in IM Lup, as presented in Fig. 6. A double-peaked line is observed, which is indicative of rotating gas disk. A similar double-peaked feature is observed in ^{12}CO J = 3–2 by van Kempen et al. (2006) using JCMT observations. However, van Kempen et al. (2006) find the line offset by ∼1 km s^{-1}. The cause of this descrepancy is unclear.

We did not find any HCO$^+$ in the direction of WW Cha. Combining our new results with those of Wilner et al. (2003), out of four targets we have two detections of HCO$^+$ and two non-detections. The statistics are yet too small to say whether the non-detections are due to the complete disappearance of gas in these disks. Data on more targets over a wider age range is required. *DL: move part of this to discussion? Add note that CO is a better tracer?*

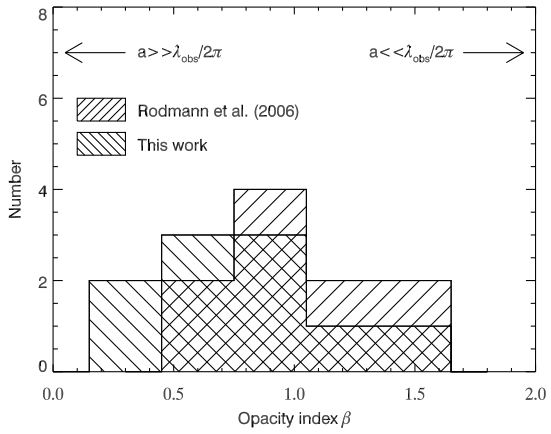

Fig. 5. Distribution of the opacity index β for the sources in our sample and those studied by Rodmann et al. (2006).

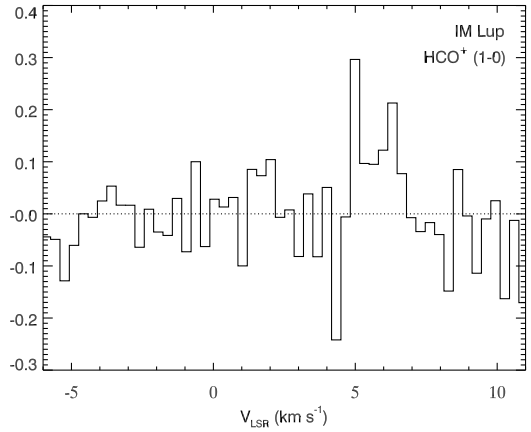

Fig. 6. HCO+ (1-0) line for IM Lup. (Binned three times. Add labels, adjust axes, make pretty... Overplot with one of Tim's lines? Wait for Olja's line?)

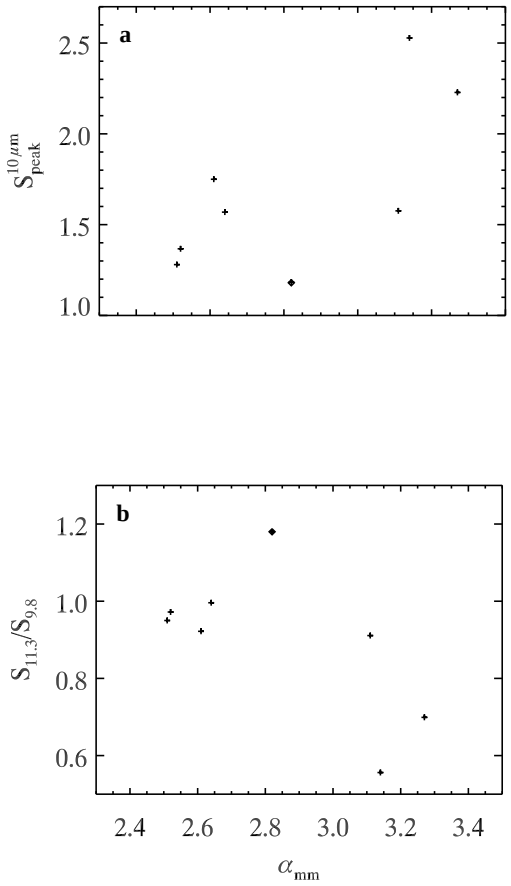

Fig. 7. Slope in the mm regime vs. the strength (upper panel) and the shape (lower panel) of the 10-μm silicate feature. The source T Cha is depicted with a diamond.

4. Discussion

4.1. Comparison with Spitzer

Whereas mm observations probe the outer disks of young stellar objects, the inner disks can be probed by infrared observations. Van Boekel (2003) and Przygodda et al. (2003) found correlations between the strength and shape of the 10-μm silicate feature, for Herbig-Ae/Be and T-Tauri stars, respectively. This trend was recently confirmed for a larger sample of T-Tauri and Herbig-Ae stars by Kessler-Silacci et al. (2006). Comparison with theoretical spectra of amorphous olivine suggest that the growth of grains weakens the 10-μm feature and changes its shape from peaked and triangular-like to plateau-like (see also Bouwman et al. 2001).

In Fig. 7 we compare the mm slope $\alpha_{\rm mm}$ as derived in Sect. 3 with the "strength" ($S^{10\mu m}_{\rm peak}$) and the "shape" ($S_{11.3}/S_{9.8}$) of the 10-μm silicate feature for those sources in our sample that overlap with the samples of Przygodda et al. (2003) and Kessler-Silacci et al. (2006). There appears to be a positive correlation between $\alpha_{\rm mm}$ and $S^{10\mu m}_{\rm peak}$ and a negative correlation between $\alpha_{\rm mm}$ and $S_{11.3}/S_{9.8}$, especially if we leave out the source T Cha, which shows emission of polycyclic aromatic hydrocarbons and may be considerably older than the other sources in the sample. Since the 10-μm feature traces the growth of grains from submicron sizes to several microns (see, e.g., Kessler-Silacci et al. 2006) and the mm slope traces the growth of grains from submm sizes to cm sizes and beyond, this may well indicate that once grain growth starts, the grains quickly grow from (sub)micron sizes to mm sizes and larger. *DL: how fast do the grains grow according to the models of Dullemond & Dominik (e.g., 2004)? How large are the differences between the time scales for the inner disk and the outer disk? Do inner and outer disk evolve separately?*

In Fig. 8 we compare $\alpha_{\rm mm}$ to the strength and shape of the 20-μm feature ($S^{20\mu m}_{\rm peak}$ and $S_{23.9}/S_{19}$, and to the spectral index over the range 13 to 35 μm, from Kessler-Silacci et al. (2006). Here we adopt their definition,

$$\alpha_{\mu\rm m} = -\frac{\log(\lambda_{\rm b}F_{\lambda_{\rm b}}) - \log(\lambda_{\rm a}F_{\lambda_{\rm a}})}{\log(\lambda_{\rm b}) - \log(\lambda_{\rm a})}, \quad (2)$$

where $\lambda_a = 13\mu$m, $\lambda_b = 35\mu$m, and F_{λ_x} is the flux density at wavelength λ_x in units of erg cm^{-2} s^{-1} μm^{-1}. Note that this corresponds to $\lambda F_\lambda \propto \lambda^{-\alpha}$, different from the definition we used for $\alpha_{\rm mm}$, $F_\nu \propto \nu^{\alpha_{\rm mm}}$. The overlap between our sample and that of Kessler-Silacci et al. (2006) is too small to draw any conclusions on the presence or absence of correlations between the mm slope and the 20-μm feature or the μm slope. (*Perhaps we should take out the comparison with the 20-μm feature, because the sample is too small to say anything. As for the comparison with the μm slope, it may be worthwhile to look at the somewhat older literature (e.g., Henning et al. 1993). To add: comparison with Herbig Ae/Be stars, e.g., Acke et al. (2004).)*

5. Conclusions

Acknowledgements. We would like to thank the ATNF for their hospitability and assistance, and specifically we would like to thank Tony Wong for extensive assistance during the observations and the data reduction. SMA staff, in particularly Alison Peck, are thanked for scheduling observations of the Lupus sources as a filler programme and for carrying out the observations. Partial support for this work was provided by a Netherlands Research School For Astronomy network 2 grant, and by an Netherlands Organisation for Scientific Research Spinoza grant.

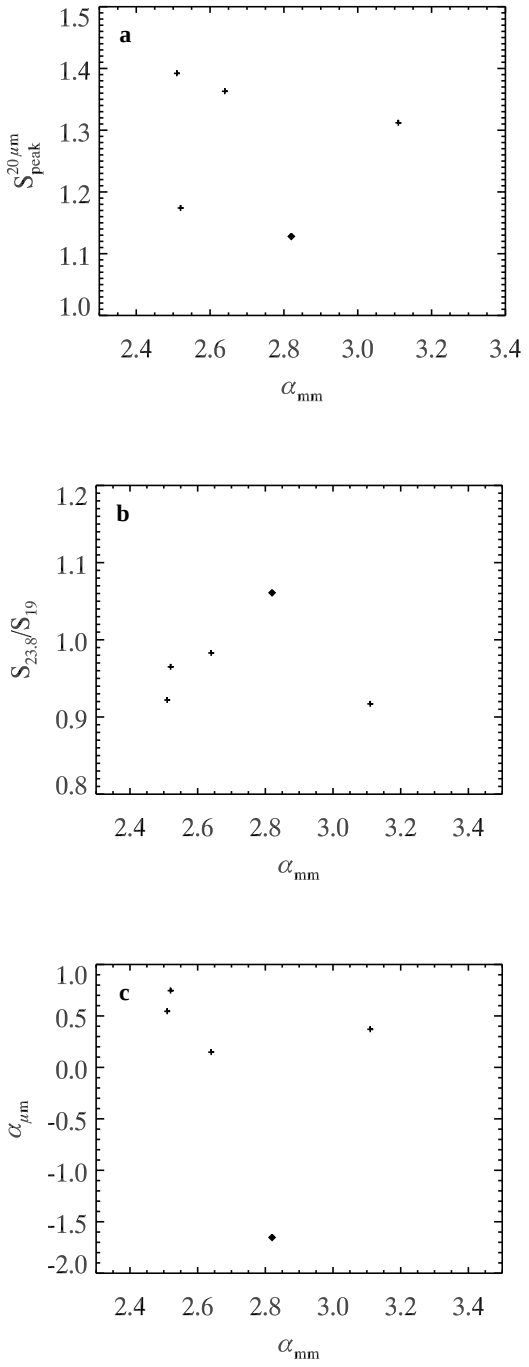

Fig. 8. Slope in the mm regime vs. the strength and shape of the 20-μm silicate feature (upper and middle panel), and the slope in the 13–35-μm range (lower panel). The source T Cha is depicted with a diamond.

References

Acke, B., van den Ancker, M. E., Dullemond, C. P., van Boekel, R., & Waters, L. B. F. M. 2004, A&A, 422, 621
Alcala, J. M., Krautter, J., Schmitt, J. H. M. M., et al. 1995, A&AS, 114, 109
Beckwith, S. V. W., Sargent, A. I., Chini, R. S., & Guesten, R. 1990, AJ, 99, 924
Bouwman, J., Meeus, G., de Koter, A., et al. 2001, A&A, 375, 950
Calvet, N., D'Alessio, P., Hartmann, L., et al. 2002, ApJ, 568, 1008
Cambresy, L., Copet, E., Epchtein, N., et al. 1998, A&A, 338, 977
Chiang, E. I. & Goldreich, P. 1999, ApJ, 519, 279
Comerón, F. in prep., in Handbook of star forming regions', ed. B. Reipurth, ASP Conf. Ser.
de Winter, D., van den Ancker, M. E., Maira, A., et al. 2001, A&A, 380, 609
Dullemond, C. P. & Dominik, C. 2004, A&A, 417, 159
Evans, N. J., Allen, L. E., Blake, G. A., et al. 2003, PASP, 115, 965
Gauvin, L. S. & Strom, K. M. 1992, ApJ, 385, 217
Henize, K. G. & Mendoza, E. E. 1973, ApJ, 180, 115
Henning, T., Pfau, W., Zinnecker, H., & Prusti, T. 1993, A&A, 276, 129
Herbig, G. H. & Bell, K. R. 1988, Catalog of emission line stars of the orion population : 3 : 1988 (Lick Observatory Bulletin, Santa Cruz: Lick Observatory, —c1988)
Herbig, G. H. & Kameswara Rao, N. 1972, ApJ, 174, 401
Hildebrand, R. H. 1983, QJRAS, 24, 267
Hughes, J., Hartigan, P., Krautter, J., & Kelemen, J. 1994, AJ, 108, 1071
Kenyon, S. J. & Gómez, M. 2001, AJ, 121, 2673
Kessler-Silacci, J., Augereau, J.-C., Dullemond, C. P., et al. 2006, ApJ, 639, 275
Kwok, S., Volk, K., & Bidelman, W. P. 1997, ApJS, 112, 557
Lawson, W. A., Feigelson, E. D., & Huenemoerder, D. P. 1996, MNRAS, 280, 1071
Malfait, K., Waelkens, C., Waters, L. B. F. M., et al. 1998, A&A,

332, L25
Natta, A., Grinin, V., & Mannings, V. 2000, Protostars and Planets IV, 559
Natta, A., Testi, L., Neri, R., Shepherd, D. S., & Wilner, D. J. 2004, A&A, 416, 179
Nuernberger, D., Chini, R., & Zinnecker, H. 1997, A&A, 324, 1036
Ossenkopf, V. & Henning, T. 1994, A&A, 291, 943
Przygodda, F., van Boekel, R., Àbrahàm, P., et al. 2003, A&A, 412, L43
Rodgers, A. W., Peterson, B. A., & Harding, P. 1978, ApJ, 225, 768
Rodmann, J., Henning, T., Chandler, C. J., Mundy, L. G., & Wilner, D. J. 2006, A&A, 446, 211
Sault, R. J., Teuben, P. J., & Wright, M. C. H. 1995, in ASP Conf. Ser. 77: Astronomical Data Analysis Software and Systems IV, 433
Shevchenko, V. S., Ibragimov, M. A., & Chenysheva, T. L. 1991, Soviet Astronomy, 35, 229
van Boekel, R., Waters, L. B. F. M., Dominik, C., et al. 2003, A&A, 400, L21
van den Ancker, M. E., de Winter, D., & Tjin A Djie, H. R. E. 1998, A&A, 330, 145
van Kempen, T. A., van Dishoeck, E. F., Brinch, C., & Hogerheijde, M. R. 2006, in prep.
Weintraub, D. A., Sandell, G., & Duncan, W. D. 1989, ApJ, 340, L69
Whittet, D. C. B., Prusti, T., Franco, G. A. P., et al. 1997, A&A, 327, 1194
Wilner, D. J., Bourke, T. L., Wright, C. M., et al. 2003, ApJ, 596, 597
Wilner, D. J., Ho, P. T. P., Kastner, J. H., & Rodríguez, L. F. 2000, ApJ, 534, L101

List of Objects

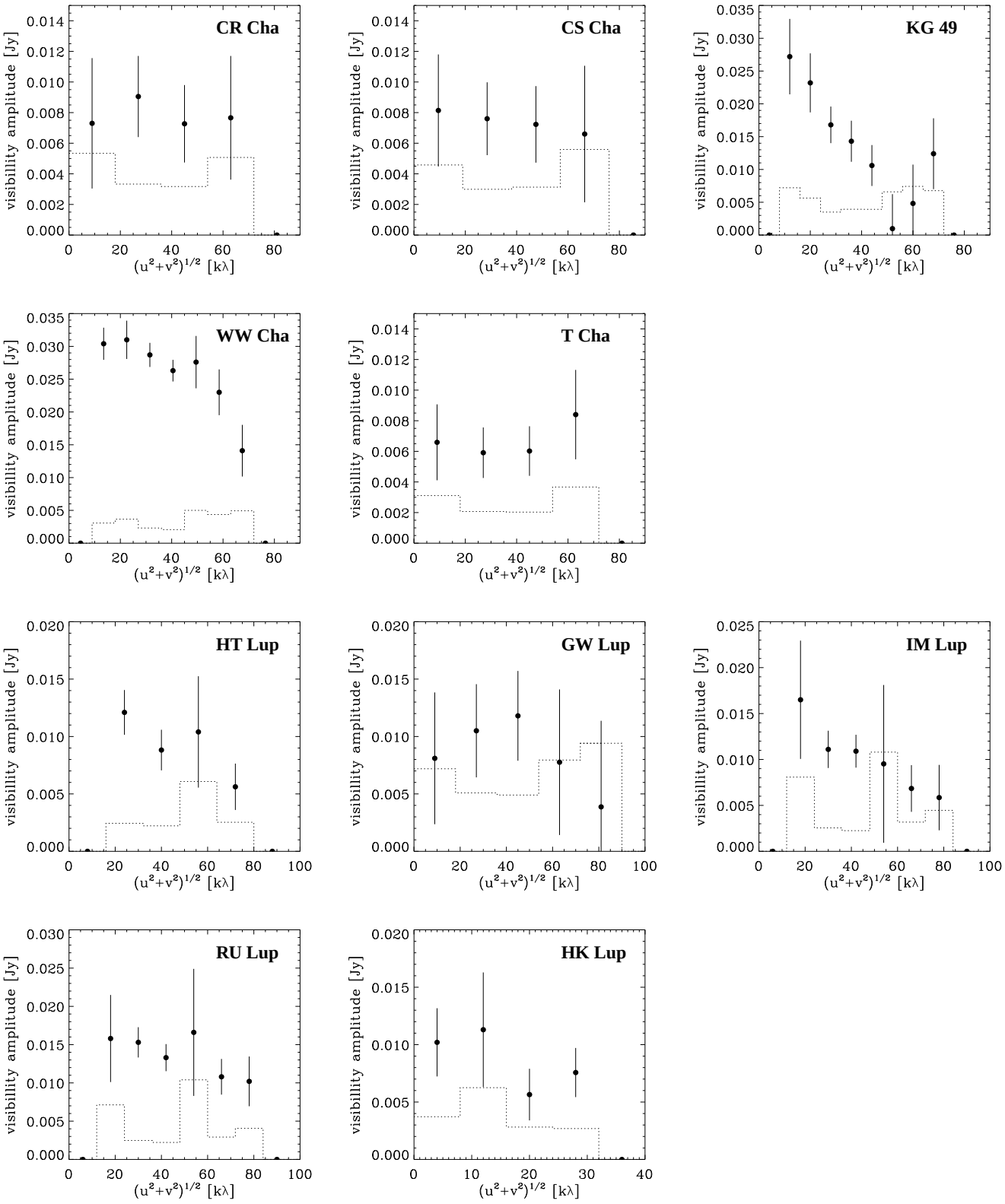

Fig. 2. Amplitude vs. (u, v) distance for sources observed with ATCA.

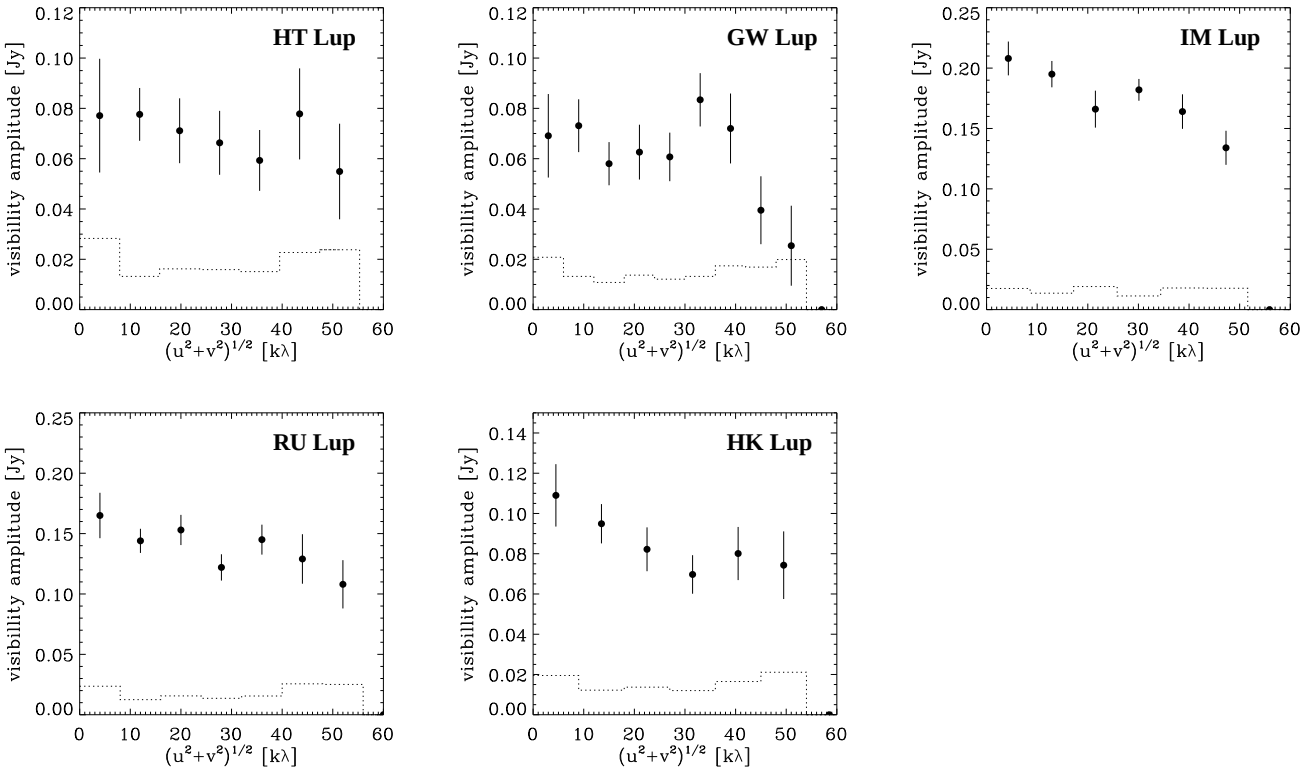

Fig. 3. Amplitude vs. (u, v) distance for sources observed with the SMA.